# CrystEngComm

Accepted Manuscript






ROYAL SOCIETY OF CHEMISTRY

www.rsc.org/crystengcomm

CrystEngComm

RSCPublishing

ARTICLE

# Facile synthesis of Pd-Pt alloy concave nanocubes with high-index facets as electrocatalysts for methanol oxidation

Cite this: DOI: 10.1039/x0xx00000x

Fangwei Zhan,[a] Ting Bian,[a] Wengao Zhao,[b] Hui Zhang,*[a] Mingshang Jin*[b] and Deren Yang[a]

Received 00th January 2012,
Accepted 00th January 2012

DOI: 10.1039/x0xx00000x

www.rsc.org/

Pd-Pt alloy concave nanocubes enclosed by high-index facets were synthesized in an ethylene glycol (EG) containing $H_2PtCl_6$ and $Na_2PdCl_4$ with ascorbic acid (AA) and KBr as reducing and capping agents, respectively. We found that a combination of bromide-induced galvanic replacement and co-reduction was responsible for the formation of these alloy concave nanocubes. The composition of the Pd-Pt alloy concave nanocubes was also tuned by varying the molar ratio of Pd to Pt salt precursors fed in the reaction. In addition, the variation in composition had a great impact on the rate of galvanic replacement, and thus the concave content of such alloy nanocrystals. These Pd-Pt alloy concave nanocubes showed the composition-dependent catalytic activity for methanol oxidation, with $Pd_{40}Pt_{60}$-based catalysts exhibiting the highest activity. Compared to the commercial Pt/C, the $Pd_{40}Pt_{60}$ alloy concave nanocubes showed much improved tolerance toward CO poisoning, together with 4.6 times enhancement in specific activity for methanol oxidation due to possible synergetic effect between Pd and Pt, and the unique surface structure associated with high-index facets.

## Introduction

Platinum (Pt) is a marvelous catalyst for a rich variety of reactions in many industrial processes and commercial devices due to its unique ability to facilitate these catalytic reactions.[1-3] For instance, Pt has been widely used in fuel-cell technology, where it acts as the most effective electrocatalyst for the electro-oxidation of fuel (e.g., methanol) at the anode and electro-reduction of oxygen at the cathode.[4] However, the catalyst made of a single Pt component can hardly meet the rapidly increasing demands of industrial applications at reduced loadings and costs due to its extremely scare abundance and sky-rocking price.[5] It is also very difficult to enhance the mass activity for this monometallic catalyst of Pt because only the outmost few layers of Pt atoms in a catalyst are actually needed in catalyzing a reaction.[6] In addition, the vulnerability toward reaction poisons (e.g., CO poison) generally occurring in the presence of pristine Pt remains serious limitations to many applications.[7,8] In order to address these issues, great efforts have been focused on the development of bimetallic structures that combine Pt with another metal that having relatively cost-effective and abundant features.[9-11] Among various metals, Pd has been identified as a promising candidate to form bimetals with Pt because they share the same face-centered cubic (*fcc*) structure and almost identical lattice constant (with a mismatch of only 0.77%).[12,13] Both the features are beneficial to the formation of bimetals with single crystallinity. Significantly, the incorporation of Pd into Pt-based bimetals can not only substantially cut the cost of the catalysts by reducing Pt loading but also extremely facilitate the enhancement or synergy of the catalytic properties due to a strong coupling between these two metals.[14,15] To this end, we have demonstrated the facile synthesis of Pd-Pt alloy nanocages with hollow interiors and their enhanced activity for the preferential oxidation (PROX) of CO relative to the catalysts made of pristine Pt.[16]

Enhancing the performance of a Pt-based catalyst, together with an attempt to reduce the loading of this precious and rare metal, also requires the use of Pd-Pt bimetals in a finely divided state with well-defined shapes.[17-19] The last decade has witnessed the successful synthesis of bimetallic nanocrystals made of Pd and Pt in a rich variety of structures and shapes.[20-24] To this end, Yang and co-workers reported the epitaxial growth of Pd layers on cubic Pt seeds to generate Pd-Pt bimetallic nanocrystals with shapes of cubes, cuboctahedrons, and octahedrons by varying the amount of $NO_2$.[25] Zheng and co-workers demonstrated that the addition of iodide ions could facilitate the replacement reaction conducted in a N,N-dimethylformamide (DMF) solution containing $Pd(acac)_2$ and $Pt(acac)_2$ under a solvothermal condition, resulting in the formation of Pd-Pt alloy nanocubes with hollow interiors.[26] Yan and co-workers demonstrated a shape-controlled synthesis of Pd-Pt alloy tetrahedrons and cubes of less than 10 nm in size through a hydrothermal process in the presence of small molecules including $Na_2C_2O_4$, KBr, and KI as capping agents.[27] Most recently, Huang and co-workers reported a facile synthesis of Pd-Pt alloy nanocrystals with well-defined shapes of octahedrons and cubes by introducing NaCl and NaI, respectively, as the capping agent.[28] Although significant progress has been made in the synthesis of Pd-Pt bimetallic nanocrystals with well-controlled shapes, most of these works only focus on the synthesis of the convex nanocrystals.

In recent years, noble-metal nanocrystals with concave surfaces have received great interest for a wide variety of catalytic and electrocatalytic applications owing to their high-index facets that having atomic steps and kinks with low coordination numbers in high densities.[29] However, synthesis of noble-metal nanocrystals with concave surfaces is still at a very early stage of development due to the involvement of high-index facets and negative surface curvature with high surface energies (the thermodynamically unfavorable one). In particular, for a bimetallic system involving Pd and Pt, there are only few reports on the synthesis of Pd-Pt bimetallic nanocrystals with a concave structure.[30,31] To this end, we have demonstrated the synthesis of Pd-Pt core-shell nanocrystals with concave surfaces through galvanic replacement between Pd nanocubes and $PtCl_6^{2-}$ in the presence of $Br^-$.[30] Despite this demonstration, we still lack a facile and effective method for the direct synthesis of Pd-Pt alloy concave nanocubes with well-controlled composition and in high yield.

Herein, we report a simple polyol approach to the synthesis of Pd-Pt alloy concave nanocubes enclosed by high-index facets including {410} and {850} through a combination of bromide-induced galvanic replacement and co-reduction process. Pd-Pt alloy concave nanocubes with different Pd/Pt atomic ratios were controllably generated in high purity by varying the molar ratios of Pd to Pt salt precursors fed in the synthesis. Owing to the high-index facet and possible synergetic effect between Pd and Pt, these concave nanocubes exhibited the substantially enhanced catalytic activity towards electro-oxidation of methanol relative to the commercial Pt/C catalysts, with $Pd_{27}Pt_{73}$ concave nanocubes being the most active one.

## Experimental

***Chemicals and materials.*** All the chemicals were used as received, including sodium tetrachloropalladate (II) ($Na_2PdCl_4$, 99.998%, Sigma-Aldrich), hexachloroplatinic acid ($H_2PtCl_6$, 99.995%, Sigma-Aldrich), Potassium tetrachloroplatinate(II) ($K_2PtCl_4$, 99.99%, Sigma-Aldrich), potassium bromide (KBr, Sinopharm Chemical Reagent Co. Ltd), poly(vinyl pyrrolidone) (PVP, MW ≈ 40000, Sigma-Aldrich), ascorbic acid (AA, Sigma-Aldrich), ethylene glycol (EG, Sinopharm Chemical Reagent Co. Ltd.), acetone (Sinopharm Chemical Reagent Co. Ltd), ethanol (Sinopharm Chemical Reagent Co. Ltd), and commercial Pt/C (20 wt% Pt on carbon black, Alfa Aesar). All syntheses were carried out in glass vials (20 mL, Shuniu).

***Synthesis of Pd-Pt alloy concave nanocubes***. Pd-Pt alloy concave nanocubes were synthesized by a combination of galvanic replacement and co-reduction in an EG solution containing $H_2PtCl_6$, $Na_2PdCl_4$, PVP, AA, and KBr. In a standard synthesis, a 6.0 mL of EG containing 200 mg of PVP, 200 mg of AA, and 150 mg of KBr was added to a vial, pre-heated to 110 $^oC$ in an oil bath under magnetic stirring for 30 min, and then ramped to 130 $^oC$. Meanwhile, 74 mg of $H_2PtCl_6$ and 54 mg of $Na_2PdCl_4$ were simultaneously dissolved into 3.0 mL of EG. After that, this EG solution was injected into the preheated vial held at 130 $^oC$ through a syringe pump with an injection rate of 2 mL/h. The reaction was allowed to proceed for 1.5 h at 130 $^oC$. The final product was collected by centrifugation, washed three times with acetone/ethanol to remove excess PVP and KBr, and re-dispersed in ethanol. We systematically investigated the effects of various parameters, including the duration of reaction, the concentration and molar ratio of $H_2PtCl_6$ and $Na_2PdCl_4$, and the type of reactants (e.g., $K_2PtCl_4$), as well as the amounts of KBr, on the morphology of resultant Pd-Pt alloy nanocrystals.

***Preparation of Carbon-Supported Catalysts.*** Carbon black (Vulcan XC-72) was used as support for making Pd-Pt catalysts (Pd-Pt/C). In a standard preparation, carbon black particles were dispersed in ethanol and sonicated for 1 h. A designed amount of Pd-Pt alloy nanocrystals were added to this dispersion with a Pd-Pt/C mass ratio of 20:80. This mixture was further sonicated for 30 min and stirred for three days. The resultant solids were precipitated out by centrifugation, washed three times with water, and re-dispersed in water.

***Morphological, Structural, and Elemental Characterizations.*** The obtained samples were characterized by X-ray powder diffraction (XRD) using a Rigaku D/MAX-ga X-ray Diffractometer with graphite monochromatized Cu Kα radiation (λ = 1.54178 Å). Transmission electron microscopy (TEM) images were taken using a JEM-1200EX microscope operated at 80 kV. High-resolution transmission electron microscopy (HRTEM) was performed using a Philips CM 200 microscope operated at 200 kV. High-angle annular dark-field scanning TEM (HAADF-STEM) and Energy dispersive X-ray (EDX) mapping analyses were taken on a Cs-corrected STEM (TitanG2 80-200 ChemiSTEM equipped with a Super-X EDX detector system), operated at 200 kV using a probe with 50 pA beam current and a converge angle of 21.4 mrad. The percentages of Pt and Pd in the samples were determined using inductively coupled plasma atomic emission spectrometry (ICP-AES, IRIS Intrepid II XSP, TJA Co., USA). X-ray Photoelectron Spectroscopy (XPS) was taken on Kratos AXIS Ultra DLD.

***Electrochemical measurements.*** The electrochemical experiments were performed at room temperature on an Autolab electrochemistry station equipped with a rotating disk electrode (RDE, No.1154-R65WHPL, 4 mm) in a thermostatic glass cell. A hydrogen electrode was used as the reference. The counter electrode was a Pt mesh (1×1 $cm^2$) connected to a Pt wire. To prepare the working electrode, 15 μL of an aqueous suspension of the catalyst was transferred to the RDE with a geometric area of 0.196 $cm^2$. Upon drying under air for 2 h, the electrode was covered with 15 μL of Nafion (Aldrich) dispersed in water (0.05%). For all of the catalysts, the metal loading on a RDE was 15.3 μg/$cm^2$. The electrodes were immersed in the nitrogen saturated 0.5 M $H_2SO_4$ solution (25 $^oC$), and the potential was scanned from 0 to 1.2V at a scan rate of 50 mV/s. The cyclic voltammograms (CVs) were used to estimate the electrochemical active surface area (ECSA) of the catalyst by calculating the hydrogen under potential desorption ($H_{upd}$) area of the catalyst. CVs for methanol oxidation were conducted in 0.5 M $H_2SO_4$ and 1.0 M $CH_3OH$ solution from 0 to 1.2 V at a scan rate of 50 mV/s. The stability was tested by chronoamperometry at 0.7 V in 0.5 M $H_2SO_4$ and 1.0 M $CH_3OH$ solution for 1000 s.

## Results and discussion

Figure 1 shows transmission electron microscopy (TEM), high angle annular dark field scanning transmission electron microscopy (HAADF-STEM), energy dispersive X-ray (EDX), and high-resolution TEM (HRTEM) images of the products prepared using the standard procedure. From the TEM image (Figure 1a), most of the nanocrystals were observed to exhibit a cubic shape with a darker contrast in the center relative to the edges, implying the formation of the concave nanocubes. The HAADF-STEM image in Figure 1b clearly shows that each face of the nanocube in the final product was excavated by a square pyramid in the center, further confirming the formation of a concave structure on the surface. The elemental distribution of Pd and Pt in the concave nanocubes was measured by EDX spectrum and mapping analysis. From the EDX spectrum (Figure S1), we can observe that four major elements were detected in the sample: Pd, Pt, C, and Cu. Obviously, Pd and Pt came from the Pd-Pt alloy concave nanocubes, while C and Cu



 

mainly originated from the carbon-coated Cu grid. The elemental mapping in Figure 1c indicates that the concave nanocubes were made of an alloy, with Pt being slightly rich on the corners and edges of the concave nanocubes. This result can be attributed to the selective galvanic replacement effect of Pt precursor on these sites, which was in agreement with our previous result.[30] The Pd-Pt alloy structure was also supported by the EDX mapping taken from an individual concave nanocube (Figure 1d). The HRTEM image of an individual alloy concave nanocube viewed along the [100] zone axis (Figure 1e) clearly shows well-resolved, continuous fringes with the same orientation, indicating that such concave nanocube is a single crystal. The angles between the facets of the projected concave nanocube and the {100} facets of an ideal cube were 14 and 32 °, which were consistent with {410} and {850} facets, respectively.[32] The structure of high-index facets (i.e., {410}) could also be determined from the arrangement of atoms on the edge-on projected face. The edge-on projected face of a Pd-Pt alloy concave nanocube in Figure 1f shows a series of alternating {400} (blue color) and {010} (red color) sub-facets, resulting in an overall profile indexed as the {410} planes. In addition, there were a number of atomic steps on the facets, which might be attractive to the catalytic reaction.

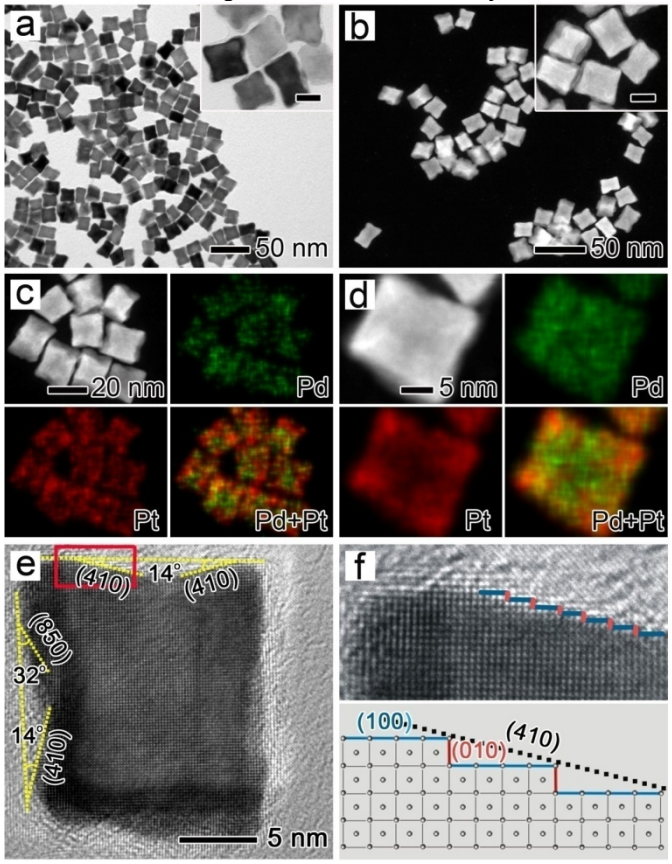


**Figure 1.** (a) TEM, (b) HAADF-STEM, (c, d) EDX mapping images of the Pd-Pt alloy concave nanocubes prepared using the standard procedure. The insets in (a, b) show the magnified images. The scale bars in these insets are 10 nm. (e) HRTEM image of an individual Pd-Pt concave nanocube viewed along the [001] zone axis. (f) Top: HRTEM image of the corner region as marked by the red box in (e), where the blue and red colors represented {400} and {010} facets, respectively. Down: The corresponding atomic model.

In order to decipher the formation mechanism of the Pd-Pt alloy concave nanocubes, we monitored the evolution of different morphologies by imaging the products obtained at different stages of a synthesis. Figure 2, a-d, shows a series of TEM images taken from the samples that were prepared using the standard procedure, except for the different period of the reactions. In the initial stage of the reaction (Figure 2a, 0.5 mL of the precursors at t = 15 min), a large number of Pd-Pt alloy nanocubes of 4-5 nm in size were obtained by co-reducing $[PdCl_4]^{2-}$ and $[PtCl_6]^{2-}$ ions with AA in the presence of $Br^-$ ions. It is clear that the formation of these nanocubes can be attributed to the preferential chemisorption of $Br^-$ ions on {100} rather than other facets.[33] As the amount of the precursors was increased to 1.0 mL (Figure 2b, t = 30 min), the nanocubes increased to 12 nm in edge length due to a co-reduction overgrowth process. Careful observation indicated that the side surfaces of these nanocubes were slightly concaved, which can be attributed to the bromide-induced galvanic replacement.[30] As such, a combination of bromide-induced galvanic replacement and co-deposition was responsible for the formation of the Pd-Pt alloy concave nanocubes. After 2.0 mL of the precursors was added (Figure 2c, t = 1 h), the product was dominated by Pd-Pt alloy nanocubes with a concave structure on the surface. When the amount of the precursors was increased to 5.0 mL (Figure 1a, t = 2.5 h), high-quality Pd-Pt alloy concave nanocubes of 17 nm in size were obtained, which was different from our previous report on the synthesis of Pd-Pt alloy nanocages.[16] We believe that the reaction rate of galvanic replacement was critical to determine the final product. Obviously, the galvanic replacement with a relatively slow rate hardly contended against the co-deposition of Pd and Pt into concave region, resulting in the formation of the nanocages and even solid nanocubes. In contrast, the faster galvanic replacement is beneficial to the concave nanocubes. Our previous study indicated that $[PtCl_6]^{2-}$ ions had a much faster rate of galvanic replacement with Pd than $[PtCl_4]^{2-}$ ions.[30] As a result, Pd-Pt alloy concave nanocubes were produced in this work when $[PtCl_6]^{2-}$ ions instead of $[PtCl_4]^{2-}$ ions serving as a reactant. This argument was confirmed by the experiment that was conducted by replacing $H_2PtCl_6$ with $K_2PtCl_4$ (Figure S2). In this case, Pd-Pt solid nanocubes were eventually obtained. In addition, this demonstration was also supported by the result with extension of the aging time to 6 h (Figure 2d), in which the concave extent of the nanocubes was greatly intensified due to the extensive galvanic replacement reaction.

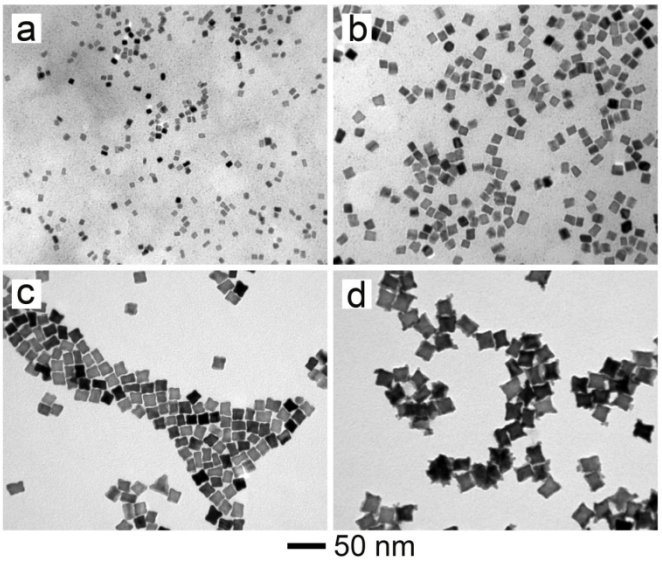


**Figure 2.** TEM images of Pd-Pt alloy nanocrystals prepared using the standard procedure, except for different period of the reactions: (a) 15 min, (b) 30 min, (c) 1 h, and (d) 6 h.

In addition to reaction time, the concentration of reagents, including the salt precursors ($Na_2PdCl_4$ and $H_2PtCl_6$) and KBr, on the effects of the final shape of Pd-Pt alloy nanocrystals were also

investigated, as shown in Figure 3. For the salt precursors ($Na_2PdCl_4$ and $H_2PtCl_6$), increasing their concentration could promote the galvanic replacement between Pd and $[PtCl_6]^{2-}$ ions, and thus favor the formation of concave structure on the surface of Pd-Pt alloy nanocubes (see Figure 3, a and b). Moreover, the concentration of KBr showed a same trend in influencing the formation of Pd-Pt alloy concave nanocubes (see Figure 3, c and d). According to our previous study,[30] a high concentration of KBr facilitated the galvanic replacement between Pd and $PtCl_6^{2-}$ ions, which was beneficial to the formation of concave nanocubes. Careful observation shows that there were a small amount of twinned structures coexisting with Pd-Pt alloy concave nanocubes when the concentration of KBr was reduced relative to that used in the standard procedure (Figure 3c). The formation of the twinned structures can be attributed to the weakened oxidative etching involved in the synthesis by decreasing the concentration of KBr.[34]

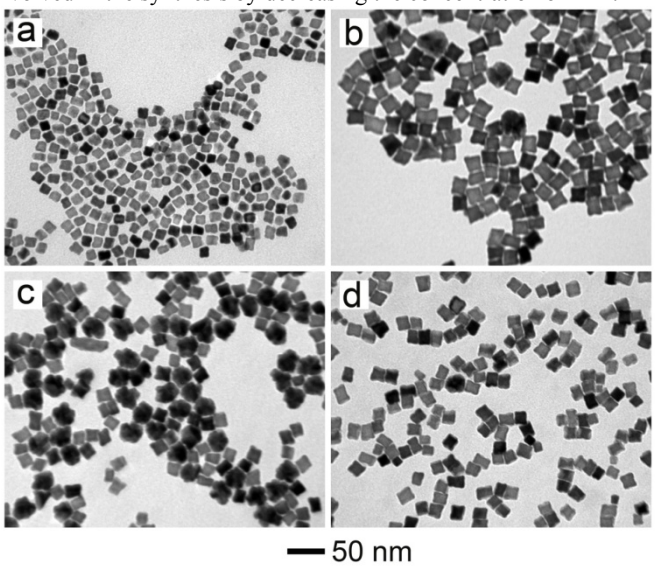


**Figure 3.** TEM images of Pd-Pt nanocrystals that were prepared using the standard procedure, except for the variation in concentration for the reagent listed below: (a) 0.03 and (b) 0.24 mmol $Na_2PdCl_4$ and $H_2PtCl_6$ with a molar ratio of 1:1; (c) 50 and (d) 800 mg KBr.

In parallel, Pd-Pt alloy concave nanocubes with controlled compositions could be readily obtained by varying the mole ratios of the Pt and Pd salt precursors supplied in the synthesis. Inductively coupled plasma atomic emission spectrometry (ICP-AES) was used to characterize the composition of the Pd-Pt alloy concave nanocubes (see Table S1). On the basis of ICP-AES analysis, $Pd_{40}Pt_{60}$, $Pd_{50}Pt_{50}$, $Pd_{66}Pt_{34}$, $Pd_{74}Pt_{26}$, and $Pd_{83}Pt_{17}$ concave nanocubes were obtained when the molar ratios between Pd and Pt precursors varied from 1:4 to 1:2, 1:1, 2:1, and 4:1. The Pd/Pt atomic ratio on the surface of these five samples was measured by XPS analysis (see Figure S3), showing the same trend as the average composition determined by ICP-AES analysis. XRD patterns (Figure S4) further confirmed that they were in an *fcc* alloy structure with the diffraction peaks slightly shifted to higher angles as compared to the standard data of pure Pt, suggesting smaller crystal parameters due to the alloying of Pt atoms with smaller Pd atoms. Figure 4 shows TEM images of these Pd-Pt alloy nanocrystals with different Pd/Pt atomic ratios. The size and shape distributions of these five samples were obtained from more than 100 nanocrystals randomly selected from TEM images (see Table S1 and Figure S5). It is clear that most of these nanocrystals exhibited the concave structure on the surface with a shape of cube. Moreover, the concave extent of the Pd-Pt alloy nanocubes was highly dependent on the molar ratios of Pd and Pt salt precursors (Figure 4, a-d). The higher proportion of $H_2PtCl_6$ in the reaction speeded up the galvanic replacement between Pd and $[PtCl_6]^{2-}$ ions, and thus favored the formation of Pd-Pt alloy nanocubes with more concave surface. As such, all the samples showed uniform size and shape distributions, except for the sample prepared with Pd/Pt molar ratio of 4/1 due to the weak galvanic replacement. Taken together, the rate of galvanic replacement reaction plays a key role in determining the final shape of Pd-Pt alloy nanocrystals.

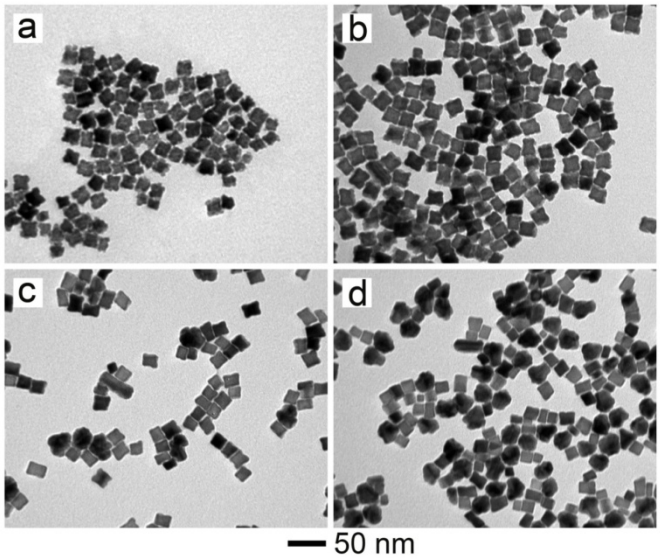


**Figure 4.** TEM images of Pd-Pt nanocrystals that were prepared using the standard procedure, except for the difference in the molar ratios of Pd to Pt salt precursors fed in the synthesis: (a) 1: 4, (b) 1: 2, (c) 2: 1, and (d) 4: 1.

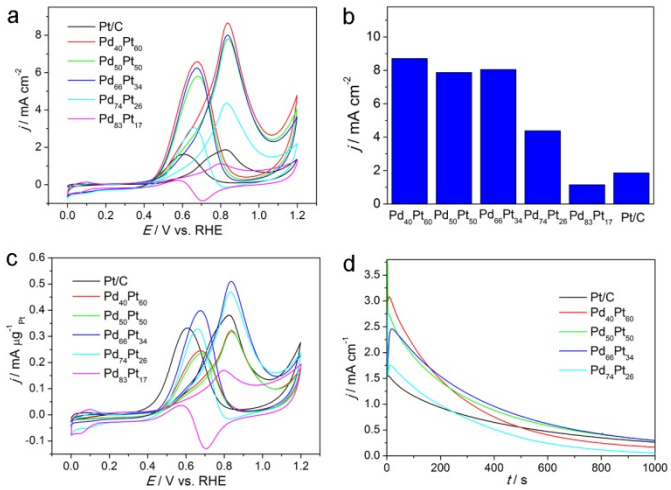


**Figure 5.** (a, b) Specific activities and (c) mass activities of the commercial Pt/C and Pd-Pt concave nanocubes with five different Pd/Pt atomic ratios for methanol oxidation that were obtained in a $N_2$-purged 0.5 M $H_2SO_4$/1.0 M $CH_3OH$ aqueous solution at a sweep rate of 50 mV/s. (d) Chronoamperometric results of methanol oxidation on the commercial Pt/C and Pd-Pt concave nanocubes with four different Pd/Pt atomic ratios.

The five alloy concave nanocubes with different Pd/Pt atomic ratios were loaded onto a carbon black support (Vulcan XC-72) and then evaluated as electrocatalysts for methanol oxidation. We benchmarked their electrocatalytic activity against the commercial

Pt/C catalyst (20 wt% of Pt nanoparticles on carbon black, Alfa Aesar). Figure S6a shows cyclic voltammograms (CVs) of these six catalysts recorded at room temperature in a $N_2$-purged 0.5 M $H_2SO_4$ aqueous solution at a sweep rate of 50 mV/s. From this CV, their electrochemically active surface areas (ECSAs) were determined by integrating the area surrounded by the hydrogen desorption curve and the baseline in the range of 0.05 - 0.4 V (see Table S1). Figure 5a compares CVs of these six catalysts for methanol oxidation at room temperature in a $N_2$-purged 0.5 M $H_2SO_4$ and 1 M MeOH aqueous solution at a sweep rate of 50 mV/s. After being normalized over the ECSAs, their peak current densities in the forward anodic scan were singled out, as shown in Figure 5b. It is clear that the specific activity increased with the percentage of Pt in the Pd-Pt alloy concave nanocubes, which was consistent with the previous result.[35] Among these catalysts, $Pd_{40}Pt_{60}$ alloy concave nanocubes showed the highest activity with a value of about 8.76 mA/cm$^2$, which was about 4.6 times higher than that of the commercial Pt/C (1.91 mA/cm$^2$). In addition, the forward ($I_f$) to backward current density ($I_b$) ratio value is generally used to evaluate the poisoning tolerance of the catalyst to the carbonaceous species.[36] Compared to the commercial Pt/C (1.2), all the Pd-Pt alloy concave nanocubes showed the higher $I_f/I_b$ ratio values (e.g., 1.4 for $Pd_{74}Pt_{26}$), indicating that the incorporation of Pd into Pt-based catalysts could alleviate the CO poisoning during the reaction. In addition, the mass activity of these catalysts (especially for $Pd_{66}Pt_{34}$) normalized by the weight of Pt was comparable to that of the commercial Pt/C in despite of their large size (see Figure 5c). The durability of the catalysts for methanol oxidation was determined by chronoamperometric experiments performed at 0.7 V for 1000 s (Figure 5d). Over the entire time range, the steady current density for the $Pd_{50}Pt_{50}$ and $Pd_{66}Pt_{34}$ catalysts was higher than that of commercial Pt/C. This enhanced performance of the Pd-Pt alloy concave nanocubes for methanol oxidation could be attributed to the bifunctional mechanism.[37] For Pd-Pt alloy catalysts, Pt was responsible for methanol dehydrogenation to form Pt-CO, whereas, Pd catalyzed the water dehydrogenation to form Pd-OH, resulting in the removal of the strongly adsorbed CO on the active sites by the reaction between Pt-CO and Pd-OH. The enhanced electrocatalytic performance of the Pd-Pt alloy concave nanocubes for methanol oxidation could also be attributed to the presence of large density of atomic steps, ledges, and kinks on the high-index facets, as well as the strong coupling between these two metals.

## Conclusions

In summary, we have developed a facile polyol approach to the synthesis of Pd-Pt alloy concave nanocubes enclosed by high-index facets, together with their compositions controlled from $Pd_{40}Pt_{60}$ to $Pd_{83}Pt_{17}$. The Pd-Pt regular nanocubes was initially formed by co-reducing $Na_2PdCl_4$ and $H_2PtCl_6$ with AA due to the selective chemisorptions of $Br^-$ ions on the {100} facets. These regular nanocubes were then excavated from the side faces due to the bromide-induced galvanic replacement between $[PtCl_6]^{2-}$ ions and Pd atoms. Meanwhile, the overgrowth at corners and edges of the nanocubes arising from the co-reduction of $[PdCl_4]^{2-}$ and $[PtCl_6]^{2-}$ ions eventually leaded to the Pd-Pt alloy concave nanocubes. The galvanic replacement at a fast rate was a key to facilitate the formation of these concave structures. Among these concave nanocubes, $Pd_{40}Pt_{60}$ alloy concave nanocubes showed the highest specific activity towards methanol oxidation, and were 4.6 times more active than the commercial Pt/C catalyst due to a combination of composition and facet effects.

## Acknowledgements

This work was supported by NSFC (No. 5137222) and Innovation Team Project of Zhejiang Province (2009R50005). M. J. would like to acknowledge supports by the start-up fund and the Fundamental Research Funds for the Central Universities of Xi'an Jiaotong University.

## Notes and references

[a] *State Key Lab of Silicon Materials, Department of Materials Science and Engineering, and Cyrus Tang Center for Sensor Materials and Applications, Zhejiang University, Hangzhou, Zhejiang 310027, P. R. China. E-mail: msezhanghui@zjue.edu.cn; FAX: +86-571-87952322; TEL: 86-571-87953190.*

[b] *Center for Materials Chemistry, Frontier Institute of Science and Technology, Xi'an Jiaotong University, Xi'an, Shaanxi 710049, P. R. China. E-mail: mingshangjin@gmail.com.*

1 A. Chen, P. Holt-Hindle, *Chem. Rev.* **2010**, *110*, 3767.
2 J. Chen, B. Lim, E. Lee, Y. Xia, *Nano Today* **2009**, *4*, 81.
3 Z. Peng, H. Yang, *Nano Today* **2009**, *4*, 143.
4 M. Debe, *Nature* **2012**, *486*, 43.
5 J. Wu, H. Yang, *Acc. Chem. Res.* **2013**, *46*, 1848.
6 N. Porter, H. Wu, Z. Quan, J. Fang, *Acc. Chem. Res.* **2013**, *46*, 1867.
7 P. Ferrin, A. Nilekar, J. Greeley, M. Mavrikakis, J. Rossmeisl, *Surf. Sci.* **2008**, *602*, 3424.
8 J. Gu, Y. Zhang, F. Tao, *Chem. Soc. Rev.* **2012**, *41*, 8050.
9 J. Wu, P. Li, Y. Pan, S. Warren, X. Yin, H. Yang, *Chem. Soc. Rev.* **2012**, *41*, 8066.
10 D. Wang and Y. Li, *Adv Mater* **2011**, 23, 1044.
11 H. Yang, *Angew. Chem. Int. Ed.* **2011**, *50*, 2674.
12 B. Lim, M. Jiang, P. Camargo, E. Cho, J. Tao, X. Lu, Y. Zhu, Y. Xia, *Science* **2009**, *324*, 1302.
13 K. Sasaki, H. Naohara, Y. Cai, Y. Choi, P. Liu, M. Vukmirovic, J. Wang, R. Adzic, *Angew. Chem. Int. Ed.* **2010**, *49*, 8602.
14 V. Stamenkovic, B. Mun, M. Arenz, K. Mayrhofer, C. Lucas, G. Wang, P. Ross, N. Markovic, *Nat. Mater.* **2007**, *6*, 241.
15 J. Nørskov, T. Bligaard, J. Rossmeis, C. Christensen, *Nat. Chem.*, **2009**, *1*, 37.
16 H. Zhang, M. Jin, H. Liu, J. Wang, M. Kim, D. Yang, Z. Xie, J. Liu, Y. Xia, *ACS Nano*, **2011**, *5*, 8212.
17 B. Lim, J. Wang, P. Camargo, C. Cobley, M. Kim, Y. Xia, *Angew. Chem. Int. Ed.* **2009**, *48*, 6304.
18 C. Serpell, J. Cookson, D. Ozkaya, P. Beer, *Nat. Chem.* **2011**, *3*, 478.
19 J. Wang, H. Inada, L. Wu, Y. Zhu, Y. Choi, P. Liu, W. Zhou, R. Adzic, *J. Am. Chem. Soc.* **2009**, *131*, 17298.
20 H. Zhang, M. Jin, Y. Xia, *Chem. Soc. Rev.* **2012**, *41*, 8035.
21 J. Wu, L. Qi, H. You, A. Gross, J. Li, H. Yang, *J. Am. Chem. Soc.*, **2012**, *134*, 11880.
22 J. Hong, S. Kang, B. Choi, D. Kim, S. Lee, S. Han, *ACS Nano* **2012**, *6*, 2410.
23 S. Guo, E. Wang, *Nano Today* **2011**, *6*, 240.
24 A. Yin, X. Min, W. Zhu, H. Wu, Y. Zhang, C. Yan, *Chem. Commun.* **2012**, *48*, 543.
25 S. Habas, H. Lee, V. Radmilovic, G. Somorjai, P. Yang, *Nat. Mater.* **2007**, *6*, 692.
26 X. Huang, H. Zhang, C. Guo, Z. Zhou, N. Zheng, *Angew. Chem. Int. Ed.* **2009**, *48*, 4808.

27 A. Yin, X. Min, Y. Zhang, C. Yan, *J. Am. Chem. Soc.* **2011**, *133*, 3816.
28 X. Huang, Y. Li, Y. Li, H. Zhou, X. Duan, Y. Huang, *Nano Lett.* **2012**, *12*, 4265.
29 H. Zhang, M. Jin, Y. Xia, *Angew. Chem. Int. Ed.* **2012**, *51*, 7656.
30 H. Zhang, M. Jin, J. Wang, W. Li, P. Camargo, M. Kim, D. Yang, Z. Xie, Y. Xia, *J. Am. Chem. Soc.* **2011**, *133*, 6078.
31 X. Xia, S. Xie, M. Liu, H. Peng, N. Lu, J. Wang, M. Lim, Y. Xia, *PNAS* **2013**, *110*, 6669.
32 J. Zhang, M. R. Langille, M. L. Personick, K. Zhang, S. Y. Li, C. A. Mirkin, *J. Am. Chem. Soc.* **2010**, *132*, 14012.
33 B. Lim, M. J. Jiang, J. Tao, P. H. C. Camargo, Y. M. Zhu, Y. Xia, *Adv. Funct. Mater.* **2009**, *19*, 189.
34 Y. Xiong, H. Cai, B. Wiley, J. Wang, M. Kim, Y. Xia, *J. Am. Chem. Soc.* **2007**, *129*, 3665.
35 Y. Liu, M. Chi, V. Mazumder, K. More, S. Soled, J. Henao, S. Sun, *Chem. Mater.* **2011**, *23*, 4199.
36 Z. Liu, X. Ling, X. Su, J. Lee, *J. Phys. Chem. B* **2004**, *108*, 8234.
37 J. Rossmeisl, P. Ferrin, G. Tritsaris, A. Nilekar, S. Koh, S. Bae, S. Brankovic, P. Strasser, M. Mavrikakis, *Energy Environ. Sci.*, **2012**, *5*, 8335.



 

## Table of Contents

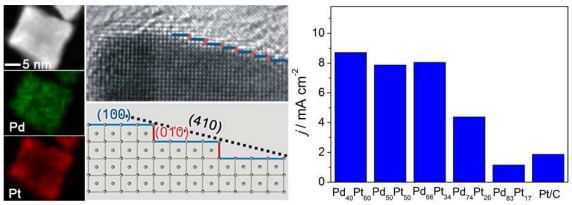


High-index faceted Pd-Pt alloy concave nanocubes with controlled compositions were generated and exhibited substantially enhanced performance for methanol oxidation.